Published in final edited form as:
*Conf Proc IEEE Eng Med Biol Soc*. 2012 ; 2012: . doi:10.1109/EMBC.2012.6346134.

# Two Solutions for Registration of Ultrasound to MRI for Image-Guided Prostate Interventions

**Mehdi Moradi**[1,2], **Firdaus Janoos**[2], **Andriy Fedorov**[2], **Petter Risholm**[2], **Tina Kapur**[2], **Luciant D. Wolfsberger**[2], **Paul L. Nguyen**[2], **Clare M Tempany**[2], and **William M Wells**[2]

Mehdi Moradi: moradi@bwh.harvard.edu

[1]Department of Electrical and Computer Engineering, University of British Columbia, Vancouver, Canada

[2]Brigham and Women's Hospital, Harvard Medical School, Boston, MA

## Abstract

Ultrasound-guided prostate interventions could benefit from incorporating the radiologic localization of the tumor which can be acquired from multiparametric MRI. To enable this integration, we propose and compare two solutions for registration of T2 weighted MR images with transrectal ultrasound. Firstly, we propose an innovative and practical approach based on deformable registration of binary label maps obtained from manual segmentation of the gland in the two modalities. This resulted in a target registration error of 3.6±1.7 mm. Secondly, we report a novel surface-based registration method that uses a biomechanical model of the tissue and results in registration error of 3.2±1.3 mm. We compare the two methods in terms of accuracy, clinical use and technical limitations.

## I. INTRODUCTION

In 2011, over 240,000 American men were diagnosed with prostate cancer [1]. A large number of these men go through diagnostic or therapeutic image-guided procedures such as biopsy or radiation treatment. Transrectal ultrasound (TRUS) is the standard imaging modality for these procedures. Ultrasound is a versatile and low cost imaging modality. However, prostate tumors do not have a visually distinct appearance in ultrasound images. As such, TRUS-guided procedures are not targeted. On the other hand, a number of imaging modalities based on Magnetic Resonance (MR) have shown promising results in visualizing prostate tumors. MR-based diffusion weighted (DW) and dynamic contrast enhanced (DCE) imaging provide quantitative measures of water molecule diffusion and blood perfusion in the tissue. Changes in the rates of both of these phenomena have been linked to progress of cancer. A number of researchers have reported the use of multiparametric MRI (mpMRI) for cancer detection in prostate with high rates of success [2], [3], [4]. It is expected that MR guidance during prostate interventions can enable targeting in biopsy and enhanced dose planning to the tumor in radiotherapy.

An example of the potential application of interventional MR guidance is in prostate brachytherapy. For low to intermediate risk prostate cancer, low dose rate brachytherapy is a widely employed radiotherapeutic option [5]. During brachytherapy, a number of radioactive sources (seeds) are implanted in the prostate region. Placement of the seeds is planned to protect the urethra and rectum and to deliver a prescribed dose to the entire prostate gland. If mpMRI evidence of cancer is present in an area, and the diagnosis can be integrated with TRUS, regional dose boosting can be implemented.

To enable interventional MR guidance, given the effect of the endorectal coil used during MR imaging and also the different patient positions between MR and TRUS image acquisitions, deformable registration is required to map the diagnostic MRI labels onto the US images. Intensity-based deformable registration of ultrasound to MRI is a challenging open problem due to the poor signal to noise ratio and lack of well defined features in ultrasound images. Therefore, contour-driven methods have been proposed [6], [7], [8], [9]. During dose planning for brachytherapy, segmentation of the prostate gland is routine, and therefore, an acceptable requirement.

We have been working towards an accurate and practical solution for MR-TRUS registration that can be used for guiding the intraprocedural dynamic dose planning during brachytherapy. To this end, we have developed two novel approaches for contour-driven registration of TRUS and T2 weighted MR images of prostate that we report here. In the first approach, we use a B-spline transform to align the binary 3D label maps resulting from manual contouring with the objective of maximizing mutual information, which is the default similarity measure in Slicer. This method is simple and fully implemented within the open source 3D Slicer environment [10]. In the second approach, we have developed a novel surface-based registration with an elastic energy penalty as the regularizer on the tissue deformation. The advantage of this method is that by assuming the tissue to be an elastic material, it provides a bio-mechanically plausible solution of the deformation throughout the internal volume of the prostate from its estimate along the prostate boundary. We applied both these methods on clinical cases and report a comparative evaluation.

## II. Methods

### A. Clinical data

The patient population consisted of those who had biopsy evidence of low to intermediate risk prostate cancer, and were candidates for low dose rate brachytherapy at Brigham and Women’s Hospital, Boston, MA. From Dec. 2011 to Feb. 2012, six patients were imaged within a HIPPA compliant study, approved by the institutional review board. All patients underwent mpMRI exams in a GE 3T MR scanner using an endorectal coil. Slice spacing was 3 mm.

The TRUS data was acquired during ultrasound volume studies performed days prior to the brachytherapy procedure. The data was acquired using a Pro Focus Ultra View 800 (BK Medical Systems, Herlev, Denmark) with the transverse array of the BK 8848 biplane transducer. For all cases the focal zone was set to 2 cm and all TGC settings were set to the middle value. The imaging protocol was to use a standard brachytherapy stepper unit and capture axial B-mode frames from base to apex, starting with the axial image at the base and retracting with 5 mm steps to cover the entire length of the gland. The 5 mm slice spacing was chosen based on the locking step size of the stepper unit. Between 8 and 12 slices covered the entire length of the gland. The contouring of the prostate images was performed in the open-source 3D Slicer 3.6.3 software package [10]. The attending radiation oncologist contoured the prostate gland on both the axial T2 weighted MRI and B-mode images of the prostate. The Model Maker module in 3D Slicer software was used to create the 3D surface meshes (smoothing iterations = 10).

### B. Approach 1: Label Map Registration

The methodology consisted of two major steps. First, we used the iterative closest point (ICP) method [11] on the prostate surface meshes in the two modalities. Second, the resulting rigid transform was used as the initial transform for deformable registration of the label maps from the two modalities obtained by manual contouring based on maximizing the

mutual information. This second step was an image-based registration approach and different from surface-based methods. We used a B-spline transform to elastically align the binary 3D label maps. We used a coarse B-spline grid to ensure that warping did not unrealistically deform the detailed features within the prostate gland.

The label map registration approach was fully implemented in 3D Slicer. The registration framework was as follows (the notation: *USS*: ultrasound surface model, *MRS*: MRI surface model, *UL*: binary label map volume acquired by contouring the gland in ultrasound, *ML*: binary label map from MRI, *MR*: grayscale MRI volume, *US*: grayscale US volume, *MRD*: binary diagnostic label map marked on MRI) and is illustrated in Figure 1:

- Use the ICP registration method to obtain a rigid transformation $(T^{r}_{MRS\rightarrow USS})$.
- Apply the ICP transform to MR labels: $\widehat{ML}=T^{r}_{MRS\rightarrow USS}\bullet ML$.
- Define a coarse B-spline grid, with cell size (distance between B-spline control points) of around half the length of the gland, on $\widehat{ML}$. We used the cell size of 30 mm.
- Use mutual information maximization [12] to obtain the following B-spline transform on binary label maps: $T^{B}_{\widehat{ML}\rightarrow UL}$.
- Obtain the transformed grayscale MR image, resampled with US image as the reference image: $\widehat{MR}=T^{B}_{\widehat{ML}\rightarrow UL}\bullet MR$.
- Re-sample the MR diagnostic map with the US image as the reference image: $\widehat{MRD}=T^{B}_{\widehat{ML}\rightarrow UL}\bullet MRD$.

The resulting $\widehat{MRD}$ was in the ultrasound image raster and was used as the diagnostic label to define cancerous and normal areas in ultrasound. $\widehat{MR}$ was used for evaluating the registration.

### C. Approach 2: Surface-Based Registration

We have developed a novel surface-based registration algorithm that combines spherical harmonic parametrization [13] of the prostate surface with a bio-mechanical model [14] of the prostate tissue to regularize the transformation between surfaces. The advantage of the spherical harmonic representation is that the registration solution now requires determining only a rotational transform that minimizes an error metric between surfaces. The outline of the method is as follows:

**a.** A mesh based surface representation of the topologically closed genus-0 prostate is generated. The mesh-representation is then conformal mapped into a spherical coordinate system with azimuthal and polar angle parameters $\theta \in [-\pi, \pi)$ and $\varphi \in [0, \pi]$, respectively. This step is done using routines provided with the Freesurfer image analysis suite [15], [16]. We denote the surface in the US and MR images by $\Gamma_{US}(\theta, \varphi) = (x(\theta, \varphi), y(\theta,\varphi), z(\theta, \varphi))$ and $\Gamma_{MR}(\theta, \varphi) = (x(\theta, \varphi), y(\theta, \varphi), z(\theta, \varphi))$ respectively.

**b.** The object enclosed by the MR surface Γmr is fit with a finite-element (FE) mesh that models it as composed of elastic material with given stiffness and compressibility parameters [14]. The tetrahedral FE-mesh has $N_e$ tetrahedra and $N_v$ vertices $\{\mathbf{v}_1, \ldots, \mathbf{v}_{N_v}\}$.

**c.** Each vertex $\{\mathbf{v}_i, i = 1 \ldots N_b\}$ on the boundary of this FE-mesh is associated with a displacement vector $\mathbf{u}_i$ for $i = 1 \ldots N_b$, which deforms it as per: $\mathbf{v}_i + \mathbf{u}_i$. Given a transformation $\mathbf{T}[\Gamma_{US}]$ of the surface $\Gamma_{US}$, this deformation $\mathbf{u}_i$ is the vector from vertex $\mathbf{v}_i$ on $\Gamma_{MR}$ to the closest point on the surface $\mathbf{T}[\Gamma_{US}]$, as per:

$$\min_{\mathbf{u}_i} \|\mathbf{v}_i + \mathbf{u}_i - \mathbf{T}[\Gamma_{US}]\|^2.$$

This can be efficiently computed using the distance map of $\Gamma_{US}$ and applying the inverse rotation to the FE-mesh representation of $\Gamma_{MR}$. The deformation vectors $\mathbf{u}_i$ for $i = 1 \ldots N_b$ are given by the evolution of the zero level-set of the fast-marching equation that is used to calculate the distance map.

**d.** Now, given $\{\mathbf{u}_i, i = 1 \ldots N_b\}$, the displacements of the internal FE-nodes of $\Gamma_{MR}$ under the linear elastic model can be determined by solving a linear system of equations [17]. The linear elastic energy for the resulting deformation is defined as $E_{el}(\mathbf{T}) = \sum_{i=1}^{N_b} \sum_{j \in \mathscr{B}_i} \mathbf{u}_i K_{ij} \mathbf{u}_j$, where $\mathscr{B}_i$ is the set of vertices adjacent to vertex $i$. Here, $K_{ij}$ is a stiffness matrix associated with each pair of FE-mesh vertices $\mathbf{v}_i$ and $\mathbf{v}_j$ and it depends on Young's modulus and Poisson's ratio of the underlying tissue.

**e.** Next, the SPHARM method [13] is used to expand the surfacea $\Gamma_{US}$, $\Gamma_{MR}$ into a complete set of spherical harmonic basis functions $Y_l^m$ of degree $l$ and order $m$ as per: $\Gamma = \sum_{l=0}^{\infty} \sum_{m=-l}^{l} c_l^m Y_l^m(\theta, \phi)$. The set of coefficients $c_l^m$ are solved for using linear least squares. In contrast to other spherical harmonic expansions, SPHARM can represent any simply connected 3D object. Moreover, the new set of SPHARM coefficients after a rotated parametrization can be directly generated from the original set, speeding up this procedure [18].

**f.** Finally, the two surfaces $\Gamma_{US}$ and $\Gamma_{MR}$ are registered by finding the rotation $\mathbf{T}_{\theta, \varphi}$ with angles $(\theta^*, \varphi^*)$ of the MR prostate surface as per:

$$(\theta^*, \phi^*) = \underset{\theta,\phi}{\operatorname{argmin}} \oint \|\Gamma_{MR}(s) - \mathbf{T}_{\theta,\phi}[\Gamma_{US}(s)]\|^2 ds + E_{el}(\mathbf{T}_{\theta,\phi})$$

Based on the orthogonality property of spherical harmonics, the first term is equivalent to the squared Euclidean distance between the SPHARM coefficients of Γmr and $\mathbf{T}_{\theta, \varphi}[\Gamma_{US}]$. The second term acts as a regularizer penalizing transformations with higher elastic energy. The optimization is performed using the Nelder-Mead method on the two rotation parameters.

**g.** Once the optimal rotation is determined, the MR image is warped into the US space by barycentric interpolation at each voxel coordinate of the deformation vectors at the vertices of the FE tetrahedron containing it.

Surface extraction, SPHARM computation and FE meshing were implemented in C++, while the optimization algorithm and image warping were implemented in MATLAB.

### D. Landmark selection and evaluation of registration error

To evaluate the registration accuracy, an expert radiologist who routinely reads prostate MRI images, contoured structures such as the verumontanum, calcifications, and cysts that were visible on both modalities. The tip of verumontanum and the geometric center of the matched calcification/cysts were used as fiducial points. In all six cases, we also used the

leftmost point on the prostate contours in the axial plane as an additional fiducial point. In total, 14 landmarks were identified from the six cases.

To evaluate the registration accuracy, we applied the estimated transformation from each method to the fiducial points. For each method, the distance from the transformed MR fiducial points to the matching ultrasound fiducial points was measured as the target registration error (TRE).

## III. Results

### A. Registration accuracy

Using the label map approach, the average TRE was 3.6 mm (0.4 mm to 5.4 mm) with a standard deviation of 1.7 mm over the 14 landmarks from the six cases. It should be noted that the identification of matching landmarks that were visible on both TRUS and MR images was challenging, particularly due to the different slice spacing in the two modalities. This limited the number of landmarks to two or three for each case.

Using the proposed surface-based registration approach, the average TRE was 3.2 mm (1.4 mm to 4.9 mm) with a standard deviation of 1.3 mm. This showed an improvement compared to the label map approach, however the increased accuracy was not statistically significant (p-value = 0.4, n=14 landmarks). Figures 2 and 3 show the results of the proposed registration method on clinical cases with the label map method and the surface-bases technique, respectively.

### B. Clinical experience

Since 3D Slicer is widely employed in the research protocols on image-guided procedures at Brigham and Women's Hospital, we chose the label map method for the clinical use. The most recent case in our study went through brachytherapy on February 23, 2012 (patient age: 73, biopsy Gleason grade: 3+4). T1, T2, DWI and DCE sequences were examined before the brachytherapy by an expert radiologist who contoured the clinical target volume defined as the areas of the prostate suspicious of cancer on T2 (low SI), raw DCE (rapid enhancement and wash out after gadolinium agent administration) and Average Diffusion Coefficient ADC (low SI) sequences. The clinical target volume, marked on MRI by the radiologist, was registered onto the axial ultrasound images and visualized in the OR using 3D Slicer. The dose in the clinical target volume was set to at least 150% of the prescribed 145 Gy dose.

## IV. Discussions and Conclusions

The surface-based method outperformed the label map approach in terms of accuracy. However, the difference was not statistically significant on the current relatively small dataset. Our choice of the label map registration approach in the brachytherapy case was mainly due to the current image guidance pipeline in our institution which uses 3D Slicer. The two methods are, however, fundamentally different in several ways. The label map registration approach deforms the interior of the prostate gland based on a B-spline transform that is solely informed by the edge information. To avoid unrealistic deformation within the gland, we employed a coarse B-spline grid. On the other hand, the surface-based registration technique uses a biomechanical model of the tissue to deform the internal structures.

Since the label map registration approach is volumetric, as opposed to surface-based, the resulting warped image is not limited to the interior of the gland. This is clear from comparison of the warped MR images in Figures 2 and 3. The restriction to deform the

image only within the surface is common to all surface-based registration techniques. In cases where the physician is interested in the position of structures outside the borders of the gland, such as the neurovascular bundle, this poses limitation for the surface-based method.

The use of the biomechanical finite element model in the surface-based registration approach results in a high computational cost. To tackle this issue, we downsampled the data to $0.6 \times 0.6 \times 3$ $mm^3$ which resulted in completion of the registration of an image pair in 30 seconds on average. This is an acceptable run time for clinical use.

The poor visibility of the prostate contour at the apex area negatively affects the registration accuracy of all contour-driven approaches, including both methods discussed here [14]. A more extensive analysis of the proposed techniques should investigate the effects of uncertainty in both contouring and landmark selection.

## Acknowledgments

This project was supported by the National Center for Research Resources and the National Institute of Biomedical Imaging and Bio-engineering of the National Institutes of Health through Grant Numbers P41EB015898 and P41RR019703, U01CA151261, and R01CA111288. Its contents are solely the responsibility of the authors and do not necessarily represent the official views of the NIH. M. Moradi received partial support from US DoD PCRP Award W81XWH-10-1-0201.

## References

1. Siegel R, Ward E, Brawley O, Jemal A. Cancer statistics, 2011: The impact of eliminating socioeconomic and racial disparities on premature cancer deaths. CA: A Cancer Journal for Clinicians. 2011; vol. 61(no. 4):212–236. [PubMed: 21685461]
2. Nagarajan R, Margolis D, Raman S, Sheng K, King C, Reiter R, Thomas MA. Correlation of gleason scores with diffusion-weighted imaging findings of prostate cancer. Advances in Urology. 2012 in Press.
3. Afnan J, Tempany CM. Update on prostate imaging. Urol Clin North Am. 2010; vol. 37(no. 21.)
4. Afaq A, Koh DM, Padhani A, van As N, Sohaib SA. Clinical utility of diffusion-weighted magnetic resonance imaging in prostate cancer. BJU International. 2011; vol. 108:1716–1722. [PubMed: 21631696]
5. Davis BJ, Horwitz EM, Lee WR, Crook JM, Stock RG, Merrick GS, Butler WM, Grimm PD, Stone NN, Potters L, Zietman AL, Zelefsky MJ. American brachytherapy society consensus guidelines for transrectal ultrasound-guided permanent prostate brachytherapy. Brachytherapy. 2012; vol. 11(no. 1):6–19. [PubMed: 22265434]
6. Daanen V, Gastaldo J, Giraud JY, Fourneret P, Descotes JL, Bolla M, Collomb D, Troccaz J. MRI/TRUS data fusion for brachytherapy. The International Journal of Medical Robotics Computer Assisted Surgery. 2006; vol. 2(no. 3):256–261. [PubMed: 17520640]
7. Haker S, Warfield SK, Tempany CM. Landmark-guided surface matching and volumetric warping for improved prostate biopsy targeting and guidance. MICCAI. 2004:853–861.
8. Hua Y, Ahmed HU, Taylora Z, Allenc C, Emberton M, Hawkes D, Barratt D. MR to ultrasound registration for image-guided prostate interventions. Medical Image Analysis. In Press, http://dx.doi.Org/10.1016/j.media.2010.ll.003.
9. Narayanan R, Kurhanewicz J, Shinohara K, Crawford ED, Simoneau A, Suri JS. MRI-ultrasound registration for targeted prostate biopsy. IEEE ISBI. 2009:991–994.
10. Pieper S, Lorensen B, Schroeder W, Kikinis R. The NA-MIC Kit: ITK, VTK, pipelines, grids and 3D slicer as an open platform for the medical image computing community. IEEE International Symposium on Biomedical Imaging: From Nano to Macro. 2006:698–701. http://www.slicer.org/.
11. Besl PJ, McKay ND. A method for registration of 3-d shapes. IEEE Transactions on Pattern Analysis and Machine Intelligence. 1992; vol. 14(no. 2):239–256.
12. Johnson HJ, Harris G, Williams K. BRAINSFit: Mutual information registrations of whole-brain 3D images, using the insight toolkit. The Insight Journal. 2007 http://hdl.handle.net/1926/1291.

13. Brechbühler C, Gerig G, Kübler O. Parametrization of closed surfaces for 3-d shape description. Comput. Vis. Image Underst. 1995 Mar; vol. 61(no. 2):154–170.

14. Risholm P, Fedorov A, Pursley J, Tuncali K, Cormack R, Wells WM. Probabilistic non-rigid registration of prostate images: Modeling and quantifying uncertainty. ISBI. 2011:553–556.

15. Dale AM, Fischl B, Sereno MI. Cortical surface-based analysis. i. segmentation and surface reconstruction. Neuroimage. 1999 Feb; vol. 9(no. 2):179–194. [PubMed: 9931268]

16. Fischl B, Sereno MI, Dale AM. Cortical surface-based analysis. ii: Inflation, flattening, and a surface-based coordinate system. Neuroimage. 1999 Feb; vol. 9(no. 2):195–207. [PubMed: 9931269]

17. Bro-nielsen M. Finite Element Modeling in Surgery Simulation, Proceedings of the IEEE. 1998; vol. 86:490–503.

18. Huang H, Shen L, Zhang R, Makedon F, Saykin A, Pearlman J. A novel surface registration algorithm with biomedical modeling applications. IEEE Trans Inf Technol Biomed. 2007 Jul; vol. 11(no. 4):474–182. [PubMed: 17674630]

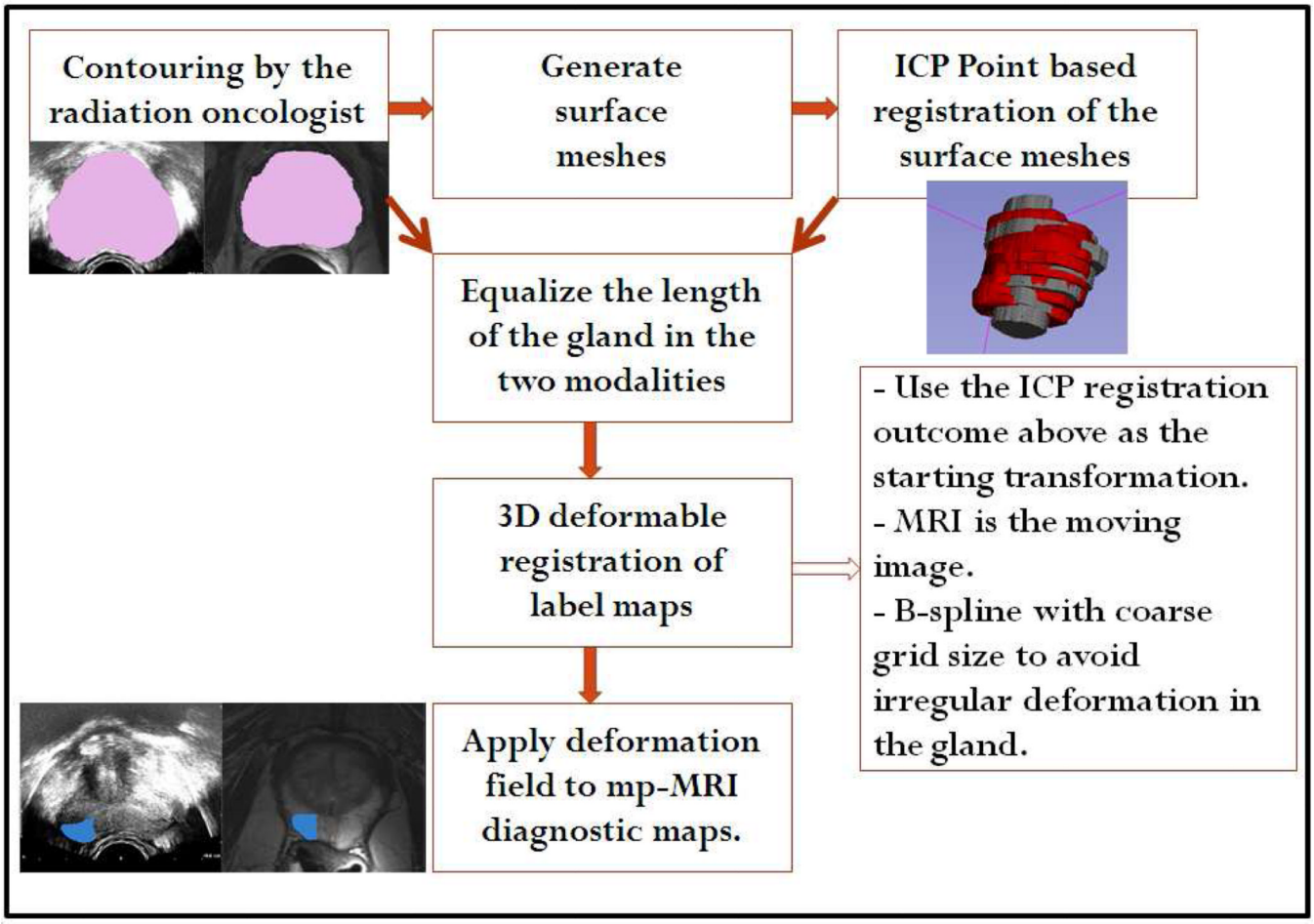


**Fig. 1.**
Workflow of the MR-TRUS registration with label map method

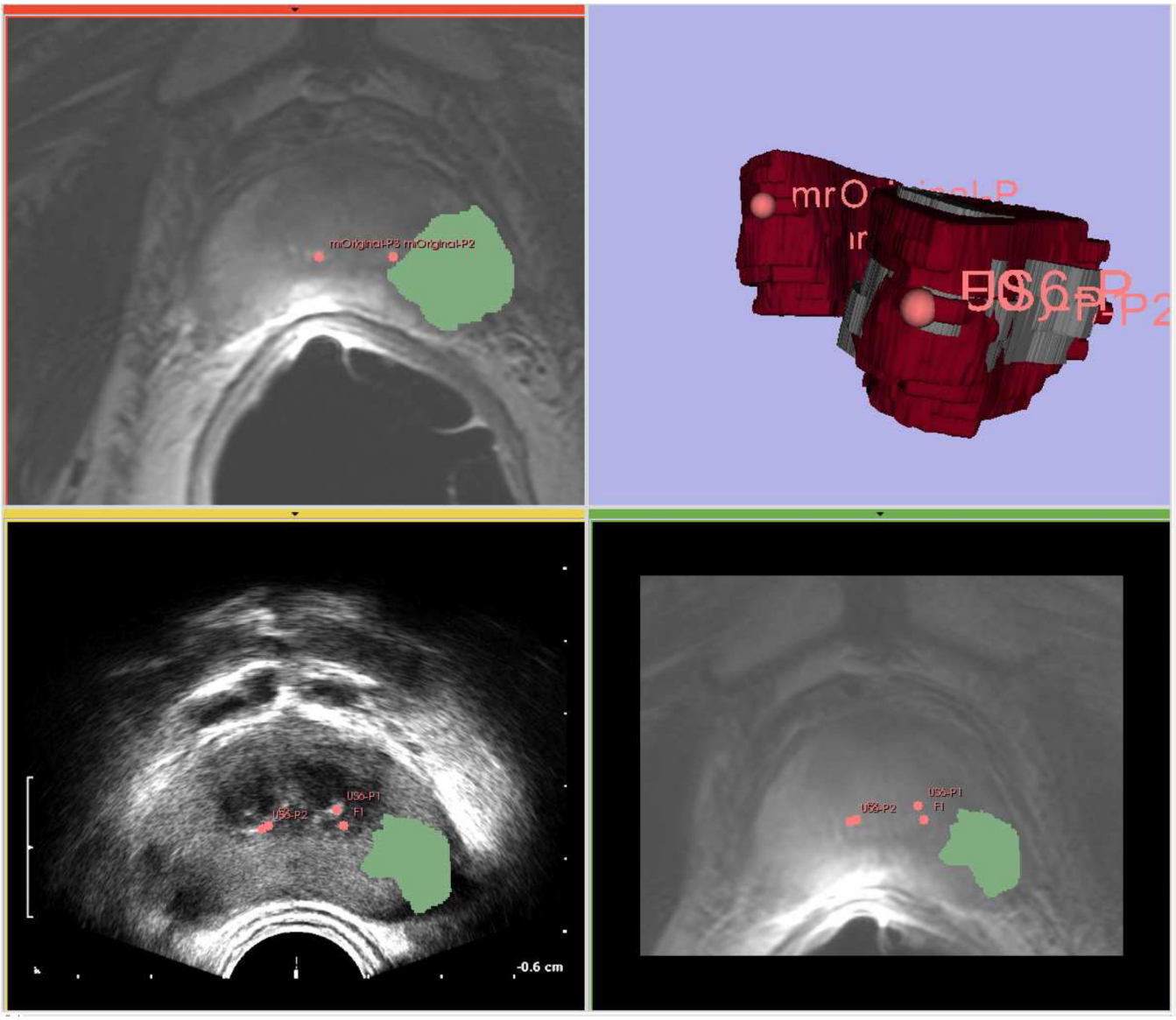


**Fig. 2. Label map registration result**

Top-right: the moving MRI surface model (red) and the fixed TRUS surface model built from manual contouring of the gland in the two modalities, registered with ICP, Top left: original MRI image with the outlined clinical target volume, and two landmarks, Bottom-right: the warped MR image and diagnostic label, Bottom-left: the resampled clinical target volume shown on the B-mode image, along with the US landmarks and the transformed landmarks from MRI.

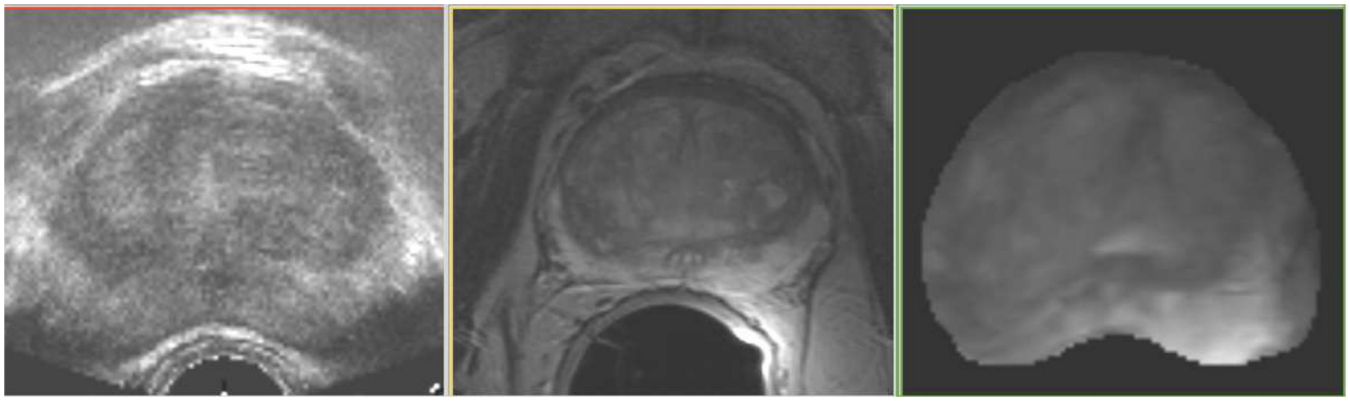

**Fig. 3. Surface-based registration result**
US (left), MR (middle) and the warped MR image (left).